Effect of two length scales on the properties of MgB_2 for arbitrary applied magnetic field

2010 J. Phys.: Condens. Matter 22 205701

(http://iopscience.iop.org/0953-8984/22/20/205701)

J. Phys.: Condens. Matter **22** (2010) 205701 (11pp) doi:10.1088/0953-8984/22/20/205701

Effect of two length scales on the properties of MgB_2 for arbitrary applied magnetic field

Madhuparna Karmakar and Bishwajyoti Dey

Department of Physics, University of Pune, Pune-411007, India

E-mail: madhu@physics.unipune.ernet.in and bdey@physics.unipune.ernet.in

Received 24 February 2010, in final form 29 March 2010
Published 26 April 2010
Online at stacks.iop.org/JPhysCM/22/205701

Abstract

Experiments carried out on the intermetallic superconducting material MgB_2 have shown anomalous magnetic field dependence of upper critical field, small angle neutron scattering form factor, specific heat, critical current etc. Similarly, scanning tunnelling microscopy (STM) experiments on vortex structures have shown unusually large vortex core size and two different magnetic and spatial field scales. Also, whereas the specific heat measurements and isotope shift experiments have shown Bardeen–Cooper–Schrieffer-like (BCS-like) behaviour, the temperature dependences of the penetration depth experiments have shown non-BCS-like behaviour. These anomalous behaviours have been attributed to the multiband superconductivity of this material and the nature of the local spatial behaviour of the magnetic induction and the order parameter components having two length scales. We report an analytical investigation of the effect of two length scales on the temperature and the applied magnetic field dependence of several properties of MgB_2, such as, the penetration depth, single vortex and vortex lattice structure, vortex core radius, reversible magnetization, critical current, small angle neutron scattering form factor and the shear modulus of the vortex lattice within the framework of two-order parameter Ginzburg–Landau theory. We solve the corresponding nonlinear Ginzburg–Landau equations numerically exactly using an iterative method for arbitrary applied field $H_{c1} < H < H_{c2}$, the Ginzburg–Landau parameter and vortex lattice symmetry. This enables us to compute the local spatial behaviour of the magnetic induction and the order parameters accurately for arbitrary applied field and a wide range of temperature. Comparison of the analytical results with experiments on MgB_2 gives very good agreement.

1. Introduction

The recent discovery of superconducting properties in the intermetallic compound MgB_2 [1] has initiated a lot of theoretical and experimental work to understand the various properties associated with this material. What has set this material apart from the existing genre of high-T_c superconductors is its simple chemical composition and its capacity to carry large critical current, while supporting a large critical temperature of $T_c = 39$ K. It is inferred from experimental studies [2, 3] that MgB_2 is an example of multiband superconductivity. Measurements of the B-isotope effect on T_c [4] have shown that superconductivity in this material is governed by strong electron–phonon coupling. The concept of multiband superconductivity was introduced more than 40 years ago [5] for materials with large disparity of the electron–phonon interaction for different pieces of the Fermi surface. *Ab initio* calculations [6] indicate that MgB_2 is a metal possessing a layered structure, with the boron atoms forming honeycombed layers and the magnesium atoms being located above the centre of the hexagons in between the boron planes. The electronic states at the Fermi level, which are responsible for the superconducting property in this material, are the σ and π-bonding boron orbitals. Since the σ-bonding orbitals are partially occupied for boron atoms, they couple very strongly to the in-plane vibrations of the boron planes, giving rise to a large energy gap of magnitude $\Delta_\sigma \approx 6.8$ meV. It is this strong electron–phonon pairing confined to the boron plane which gives a major contribution to the superconducting property of this material. Apart from this, a weak contribution is obtained

from the π-bonding states present in the remaining parts of the Fermi surface, which gives rise to a smaller energy gap of magnitude $\Delta_\pi \approx 1.8$ meV. The experimental efforts have led to the consensus that in MgB_2 the superconductivity is mainly driven by the σ-band and its interband coupling with the π-band induces a small superconductivity in the π-band [7, 8].

Experiments have demonstrated several new and interesting properties associated with the two-band nature of this material. It has been found that the anisotropy of the upper critical magnetic field shows anomalous temperature dependence [9] while the lower critical magnetic field is almost isotropic, indicating that in MgB_2 the coherence length and penetration depth anisotropy $\Gamma = \xi_{ab}/\xi_c = \lambda_c/\lambda_{ab}$ is field dependent and rises from an isotropic value ($\Gamma \approx 1$) at the lower magnetic field to an anisotropic value ($\Gamma \approx$ 5–6) at the higher magnetic field. Point contact [10] and small angle neutron scattering (SANS) measurements [11] have suggested that anomalous magnetic field dependence contributes towards the anisotropic property of the material. Above some cross-over magnetic field of $H \approx 0.1$ [12] the contribution of the π-band is suppressed by the magnetic field and the anisotropy of the material is then governed by the two-dimensional σ-bands. Below this cross-over magnetic field the three-dimensional π-bands plays a dominant role in determining not only the anisotropy but also other properties of this material. The anomalous magnetic field dependence of the contribution of the two bands has also been observed in other experimentally observable properties. The kink observed in the magnetic field dependence of the Sommerfeld coefficient [13] arises due to the rapid suppression of the contribution of the π-bands with increasing magnetic field. Moreover, the form factors in small angle neutron scattering (SANS) experiments [11], muon spin relaxation rate [14] and the logarithmic derivative of the reversible magnetization [14], which are all expected to be proportional to $1/\lambda^2$, show anomalous magnetic field dependence. Recent scanning tunnelling microscopy (STM) studies [15] have supported the presence of two-order parameter components in the MgB_2 superconductor.

The multiband scenario of the MgB_2 superconductor has also been modelled in theoretical studies. While some of the microscopic theories were based on the σ or σ–π-band scenarios for superconductivity [16, 17], others are based on the π-band model of superconductivity [18]. Koshelev *et al* [19] has studied the vortex state of MgB_2 by solving the two-band Usadel equations. Zhitomirsky *et al* [20] have studied a two-band Ginzburg–Landau (GL) theory but the study is restricted to the applied magnetic field regions near the upper (H_{c2}) and lower (H_{c1}) critical magnetic fields (where the nonlinear GL equations are approximated as linear) and hence cannot describe the anomalous dependence of the properties of MgB_2 on the applied field. They have obtained the single vortex and vortex lattice structure. Betouras *et al* [21] have used the two-band GL theory to study the effect of pressure on the MgB_2 superconductor. In a recent paper, Klein *et al* [22] showed that the anomalous applied field dependence of the properties of MgB_2 can be explained if one *assumes* that the penetration depth and the coherence length are field dependent. Another limitation of the earlier two-band GL theories is the approximation of expressing one of the order parameters in terms of the other, thereby reducing it to an effective one-order parameter GL theory [22, 23].

In this paper we study the superconducting properties of MgB_2 superconductor in the framework of a two-order parameter GL theory. We solve the coupled nonlinear GL equations involving the two-order parameters and the magnetic induction by a numerically exact iteration technique in two spatial dimensions [24]. The justification for carrying out the numerical computation in two-dimensions is due to the fact that the superconductivity in MgB_2 is principally governed by the two-dimensional σ-bands. Experimental observations [12] have suggested that up to an applied magnetic field of $H \approx 0.1$ T the two-dimensional σ-bands dominate the superconducting properties of MgB_2 and below this the three-dimensional π-band tends to be predominant. Since we are interested in studying the anomalous magnetic field dependence on the properties of the MgB_2 we need to study the intermediate region of the applied magnetic field where the GL equations are not linear. We therefore do not linearize the coupled nonlinear GL equations. Also we have not used any ansatz to express one of the order parameter components in terms of the other. Thus, we solve the fully coupled nonlinear GL equations over the entire range of the applied magnetic field for arbitrary vortex lattice symmetry and wide temperature range. We also do not assume any dependence of the penetration depth and the coherence length on the applied field, as was done in earlier studies [22]. In fact we show that this dependence comes out of our calculations. The local spatial behaviours of the order parameter and magnetic field such as the widths of the order parameter and magnetic field profiles and their variation with arbitrary magnetic field induction and temperature have been explored in detail. The changes in the local spatial behaviours are reflected on the experimentally observable quantities such as the vortex core radius and the penetration depth of the magnetic induction. We have also calculated the reversible magnetization, superconducting current density and small angle neutron scattering (SANS) form factor which depends on the local spatial behaviour of order parameters and the magnetic field. Since our numerical method is valid for arbitrary vortex lattice symmetry, it enables us to determine the shear modulus of the vortex lattice which gives a measure of the strength of the vortex lattice and is of importance to understand the melting of the flux line lattice at high temperatures. Though not as pronounced as in the case of the high-T_c superconducting cuprates in which thermal fluctuation effects are predominant near T_c, recent studies [25] have shown that the melting of the vortex lattice is important for MgB_2 superconductors also.

The paper is organized as follows, in section 2 we discuss the theoretical formalism along with the numerical method involved in the work, section 3 deals with the results obtained from our calculations and their analysis and finally in section 4 we conclude with suggestions for future work.

2. Theoretical formalism and numerical calculations

The two-dimensional average GL free energy density functional for MgB_2 superconductor is given as [20, 21],

$$f = \Big\langle \alpha_\sigma|\psi_\sigma|^2 + \alpha_\pi|\psi_\pi|^2 + \beta_\sigma|\psi_\sigma|^4 + \beta_\pi|\psi_\pi|^4 + \gamma(\psi_\sigma^*\psi_\pi + \psi_\sigma\psi_\pi^*) + \frac{1}{2m_\sigma}|\mathbf{\Pi}\psi_\sigma|^2 + \frac{1}{2m_\pi}|\mathbf{\Pi}\psi_\pi|^2 + \gamma_1(\Pi_x\psi_\sigma\Pi_x^*\psi_\pi^* + \Pi_y\psi_\sigma\Pi_y^*\psi_\pi^* + \text{c.c}) + \frac{1}{8\pi}(\nabla\times\mathbf{A})^2\Big\rangle. \quad (1)$$

On symmetry grounds, various types of interaction in quartic and gradient terms between the two superconducting order parameters are possible and have been considered in the literature [20, 21, 26, 27]. In the above free energy density functional ψ_σ and ψ_π are the two-order parameter components, corresponding to the σ and π-bands respectively, $\mathbf{\Pi} = -i\hbar\nabla - 2e/c\mathbf{A}$ is the momentum operator. $\mathbf{A}$ is the vector potential and is related to the local magnetic field as $\mathbf{B} = \nabla\times\mathbf{A}$. The magnetic field is applied along the z-direction, i.e. $\mathbf{B} = B\hat{z}$. α_σ and α_π are temperature dependent quantities and can be expressed as, $\alpha_i = \alpha'(T - T_i)$ where $i = \sigma, \pi$. The β-coefficients have positive values, γ is the linear interband coupling parameter while γ_1 is the mixed gradient interband coupling parameter. The most important parameter of this formalism is the linear interband coupling parameter γ which gives the coupling between the σ and π-band order parameter components. For $\gamma < 0$, a stable phase with a phase difference of 0 between the order parameter components is realized and for $\gamma > 0$ a phase difference of π between the order parameter components is stable. The coupling between the order parameter components is thus primarily governed by the linear interband coupling parameter γ. This is unlike the case of the high-T_c cuprates where due to the tetragonal symmetry of the material the mixed gradient coupling term is mainly responsible for the superconducting properties. The GL free energy density functional (equation (1)) can be rewritten in the dimensionless form as

$$f = \langle -\omega_\sigma + (1/2){\omega_\sigma}^2 + \alpha\omega_\pi + \beta_\pi\omega_\pi^2 + 2\gamma\cos(\phi)(\omega_\sigma\omega_\pi)^{1/2} + g_\sigma + \omega_\sigma Q^2 + M_1 g_\pi + M_1\omega_\pi Q^2 + 2M_2[\cos(\phi)(Q^2(\omega_\sigma\omega_\pi)^{1/2} + (\nabla\omega_\sigma)(\nabla\omega_\pi)/4\kappa^2(\omega_\sigma\omega_\pi)^{1/2}) + \sin(\phi)/2\kappa \times (\mathbf{Q}(\nabla\omega_\pi)(\omega_\sigma/\omega_\pi)^{1/2} - \mathbf{Q}(\nabla\omega_\sigma)(\omega_\pi/\omega_\sigma)^{1/2})] + (\nabla\times\mathbf{Q})^2\rangle \quad (2)$$

where, the order parameter components are expressed in terms of the gauge invariant real quantities as $\psi_\sigma(x, y) = \sqrt{\omega}_\sigma(x, y)\exp[i\phi_\sigma(x, y)]$ and $\psi_\pi(x, y) = \sqrt{\omega}_\pi(x, y)\exp[i\phi_\pi(x, y)]$, $\kappa = \lambda/\xi$ is the GL parameter, $\mathbf{Q} = \mathbf{A} - \nabla\phi/\kappa$ is the gauge invariant supervelocity of the electrons and $g_i = (\nabla\omega_i)^2/4\kappa^2\omega_i$ with $i = \sigma, \pi$. In this equation we have expressed the coefficients of the various terms of equation (1) in terms of reduced units as, $\alpha = \alpha_\pi/|\alpha_\sigma|$, $\beta_\pi = \beta_\pi/2\beta_\sigma$, $\gamma = \gamma/|\alpha_\sigma|$, $M_1 = m_\sigma/m_\pi$, $M_2 = \gamma_1/(1/2m_\sigma)$. The local magnetic field is rescaled as $\mathbf{B} = \mathbf{B}/\sqrt{2}H_c$ in terms of the thermodynamic critical field H_c, while the order parameter components and the free energy density are expressed in units of $|\alpha_\sigma|/2\beta_\sigma$ and $|\alpha_\sigma|^2/2\beta_\sigma$ respectively. Since the coupling between the order parameter components is primarily governed by the linear interband coupling parameter γ, for our calculation we have set the other coupling parameter, namely the mixed gradient interband coupling parameter M_2, to be equal to zero. For the sake of completeness we have, however, checked the effect of the mixed gradient interband coupling parameter M_2 on the various properties of MgB_2 and no significant effect has been observed. Among the five other parameters in the free energy density functional (equation (2)) namely α, β_π, γ, M_1 and κ, the parameters α and β_π are determined by using the relations given in [20]. Also from [20] we determine $M_1 = K_2/K_1 \approx 1.06$. For the GL parameter κ, we have used the experimentally determined value of $\kappa = 6.4$ [22, 28]. The only free parameter in the formalism is thus the linear interband coupling parameter γ which is determined by fitting the reversible magnetization results obtained by our model with the corresponding experimental data.

The coupled nonlinear GL equations corresponding to the free energy density functional (2) are obtained by minimizing the free energy density functional with respect to the order parameter components $\omega_s(\mathbf{r})$, $\omega_d(\mathbf{r})$ and the supervelocity $\mathbf{Q}(\mathbf{r})$. The coupled nonlinear equations in magnetic induction and the two order parameters are solved by using a numerically exact iteration technique with 16 digit accuracy [24].

3. Results and discussions

The solutions of the coupled nonlinear GL equations thus obtained are then used to study the various properties of MgB_2 over the entire range of applied magnetic field and a wide range of temperature and compared with experiments.

3.1. Vortex lattice structure

The vortex positions are given by $\mathbf{R} = \mathbf{R}_{mn} = (mx_1 + nx_2, ny_2)$ (m, n integer) and $\mathbf{K} = \mathbf{K}_{mn} = (\frac{2\pi}{x_1 y_2})(my_2, nx_1 + mx_2)$. For the triangular lattice, one has $x_2 = x_1/2$, $y_2 = x_1\sqrt{3}/2$, and for the square lattice $x_2 = 0$, $y_2 = x_1$ [24]. We start by determining the dependence of the free energy density $f(x_2 = x_1/2, y_2)$ on the lattice parameter y_2 and find the value of y_2 for which the free energy is minimum. The value of y_2 corresponding to the minimum of free energy suggests the stable structure of the vortex lattice. For the MgB_2 superconductor we obtain a triangular vortex lattice. This result agrees with several band structure calculations [29] and experimental [11] results which suggest a triangular vortex lattice for MgB_2. Figure 1 shows the triangular vortex lattice structure of MgB_2, where we have plotted the contour plots for the order parameter components $\omega_\sigma(x, y)$, $\omega_\pi(x, y)$ and the magnetic field $B(x, y)$.

3.2. Local spatial behaviours

3.2.1. Order parameters. The important aspect of the present work is to study the local spatial behaviour of the

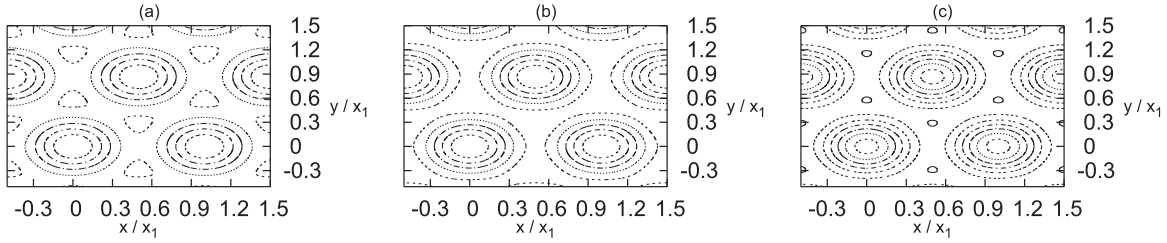

Figure 1. Contour plots for (a) $\omega_\sigma(x, y)$, (b) $\omega_\pi(x, y)$ and (c) $B(x, y)$. The parameter values used are $\alpha_\pi/|\alpha_\sigma| = 0.66$, $\beta_\pi/2\beta_\sigma = 0.75$, $\gamma = \gamma/|\alpha_\sigma| = -0.1$, $M_1 = 1.06$, $\kappa = 6.4$ and $b = B/H_{c2} = 0.8$.

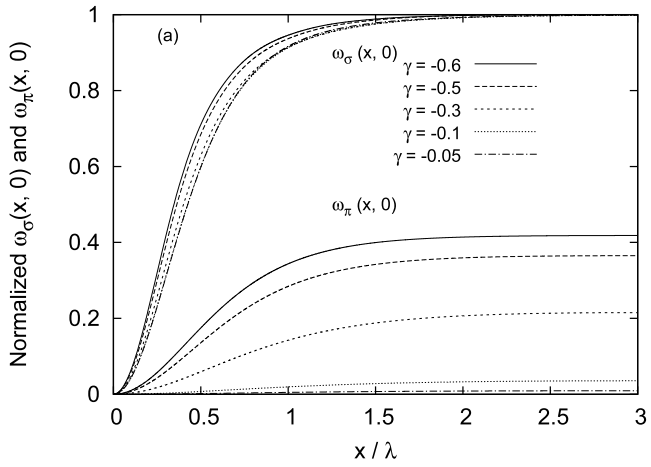

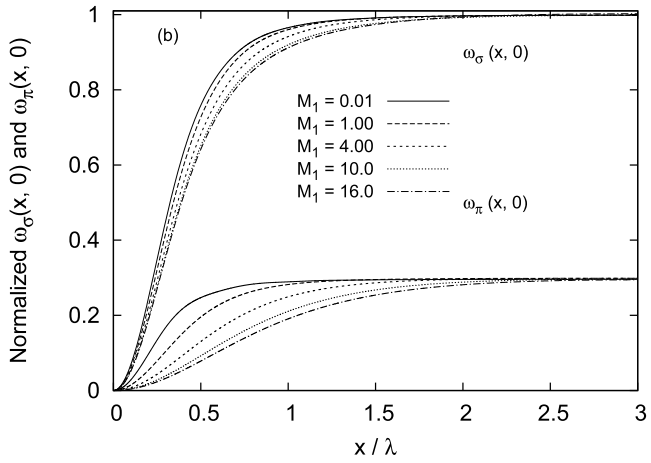

Figure 2. Variation of normalized superconducting order parameter profiles for different values of (a) the linear interband coupling parameter γ and (b) the coupling parameter M_1. The parameter $b = 0.005$ and $T/T_\sigma = 0.3$. For (a) $M_1 = 9.0$ and for (b) $\gamma = -0.4$.

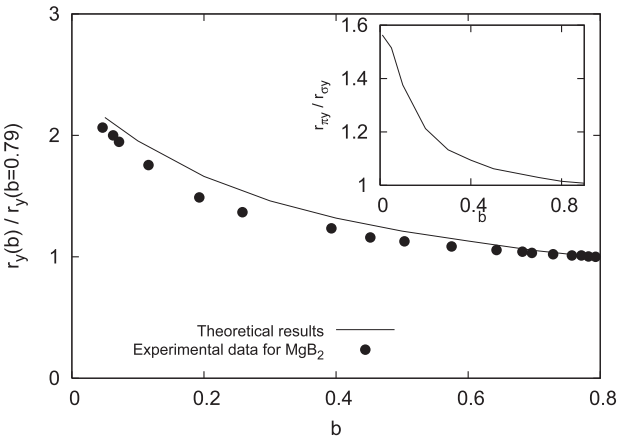

Figure 3. A comparison between the experimental data [22] and the theoretical results of the magnetic field dependence of the vortex core radius. The other parameter values are the same as in figure 1. The inset shows the magnetic field dependence of the relative vortex core radius of σ- and π-band order parameter components.

order parameter components and magnetic field. The widths of the order parameter and magnetic field profiles, which we obtain from the local spatial behaviour, correspond to experimentally observed properties such as the vortex core radius and penetration depth of the magnetic field respectively. As has been mentioned above, the magnetic field dependence of the various properties of this material can be explained by understanding the magnetic field dependence of the vortex core radius and penetration depth.

Figure 2(a) shows the plots of the σ and π-band order parameter components $\omega_\sigma(x, 0)$ and $\omega_\pi(x, 0)$ normalized to the saturation value of $\omega_\sigma(x, 0)$ for different values of the linear interband coupling parameter γ. The figure clearly shows that there is significant difference in the spatial variation of the magnitude and width of the order parameter components, with the π-band order parameter component varying spatially more slowly as compared to that of the σ-band. The differences in the core size of the two order parameter components indicate that there are two different length scales, ξ_σ and ξ_π, over which the order parameter components vary. This observation is similar to that discussed in [20] where the single vortex structure is studied in the absence of magnetic field. From figure 2(a) we can see that for variation of the coupling parameter γ from -0.6 to -0.05, the magnitude of the π-band order parameter is reduced by a factor of $\sim$40 while the corresponding vortex core radius increases by a factor $\sim$2. On the other hand, the spatial variation of the σ-band order remains almost unchanged with variation of the parameter γ. This difference in the spatial behaviour of the order parameter components is also seen in their variations with coupling parameter M_1, as shown in figure 2(b). An interesting feature that can be observed from this figure is that the size of the vortex core corresponding to the weakly superconducting π-band order parameter component is larger than that of the σ-band. This is a characteristic feature of the two-band superconductors [19]. Figure 3 shows the

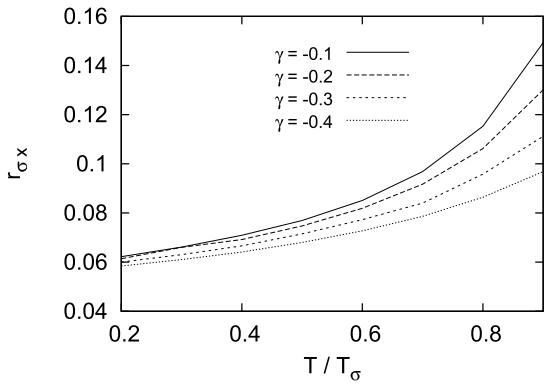

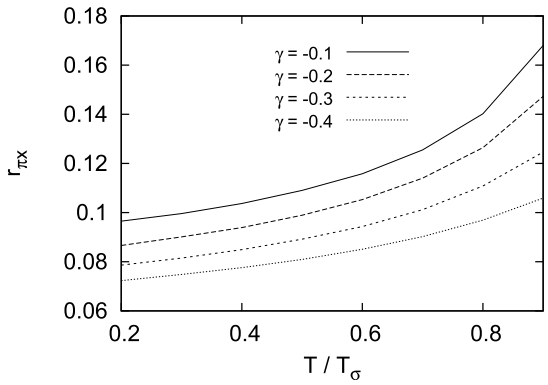

Figure 4. Temperature dependence of the theoretical vortex core radius for different values of the linear interband coupling parameter γ. Parameter $b = 0.01$ and the other parameter values are the same as in figure 1.

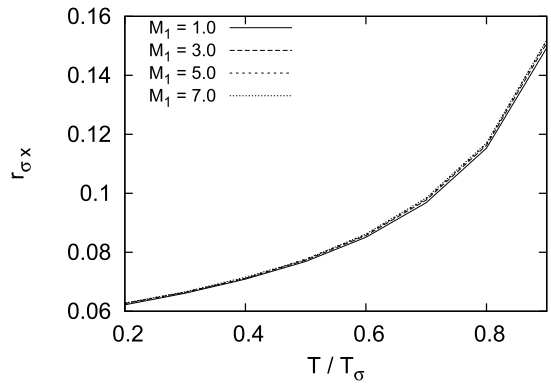

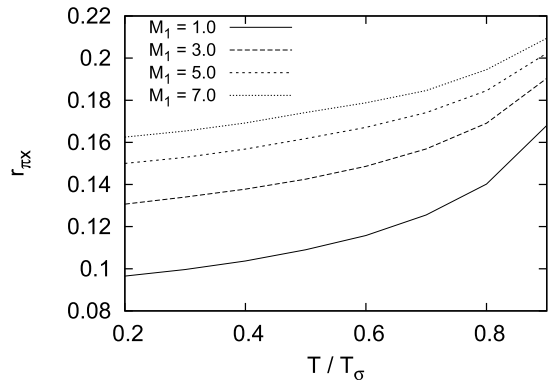

Figure 5. Temperature dependence of the theoretical vortex core radius for different values of the coupling parameter M_1. Parameter $b = 0.01$ and the other parameter values are the same as in figure 1.

comparison between the analytical result and the experimental data [22] for the magnetic field dependence of the vortex core radius of MgB_2. In this plot the vortex core radii have been measured as the FWHM of the order parameter components along the y-axis. Similar results are obtained for the x-component also. The combined vortex core size as plotted is defined as $r_y = 2r_{\sigma y} + r_{\pi y}$, which gives the best fit with the experimental results. The inset of the figure shows the magnetic field dependence of the relative vortex core size of the σ- and π-band order parameter components ($r_{\pi y}/r_{\sigma y}$). For all magnetic field inductions the vortex core size corresponding to the π-band exceeds that of the σ-band and this behaviour is more prominent at lower magnetic field regimes.

Figure 4 shows the temperature dependence of the vortex core radii for the σ- and π-band order parameter components. The vortex core radius for both the order parameter components decreases with decrease of temperature. For any value of the coupling parameter γ the size of the vortex core corresponding to the π-band order parameter component always exceeds that of the σ-band. The observation of the shrinkage of the vortex cores corresponding to both the σ and π-band order parameter components with temperature in MgB_2 is consistent with previous theoretical works [30, 31] and has been attributed to the fact that the shrinkage of the vortex core in the π-band is induced by that in the σ-band and thus the size of the vortex core corresponding to the π-band always exceeds that of the σ-band. Figure 5 shows the temperature dependence of the vortex core radius for different values of the parameter M_1. In this case also shrinkage of vortex core radius with decreasing temperature is observed for all values of the parameter M_1. However, the variation of the σ and π-band vortex core radius with the parameter M_1 is very different. Whereas, for the σ-band the variation is almost negligible, for the π-band it is more prominent.

3.2.2. Magnetic field. We now study the local spatial behaviour of the magnetic field profile. The width of the magnetic field profile gives a measure of the penetration depth (λ). We study the magnetic field as well as the temperature dependence of the penetration depth for different values of the coupling parameters γ and M_1.

Figure 6 shows the plot of the calculated magnetic field dependence of the penetration depth with the experimental data obtained from superconducting quantum interference device (SQUID) measurements [14]. The figure also shows the comparison of our analytical results with the analytical results obtained using an effective single-order parameter model [22]. Whereas in [22] it is assumed that the coherence length and the penetration depth is dependent on the applied field, we compute the actual dependences analytically, which are as shown in figures 3 and 6, respectively. It has been suggested [22] that the results obtained from the SQUID measurements indicate a penetration depth value of

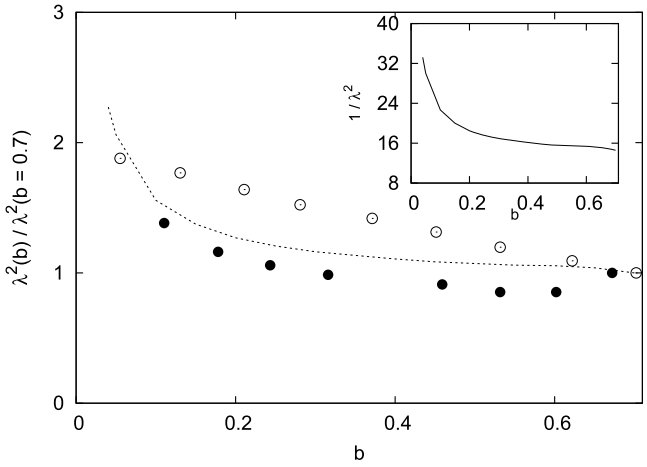

Figure 6. A comparison between the theoretical magnetic field dependence of the penetration depth with the experimental data obtained from SQUID measurements [14] (closed circles) and the results obtained from the single-band model [22] (open circles). The parameter values used for the theoretical calculation are the same as in figure 1. The inset shows the magnetic field dependence of the inverse square of the penetration depth.

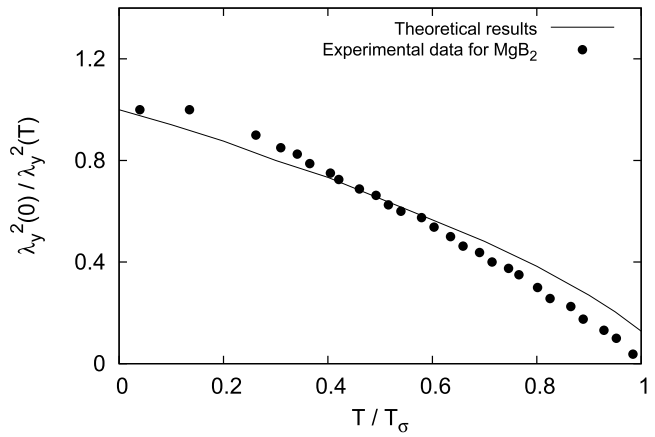

Figure 7. A comparison between the theoretical and experimental data [32] of the temperature dependence of the penetration depth. Parameter $b = 0.003$ and other parameter values are the same as in figure 1.

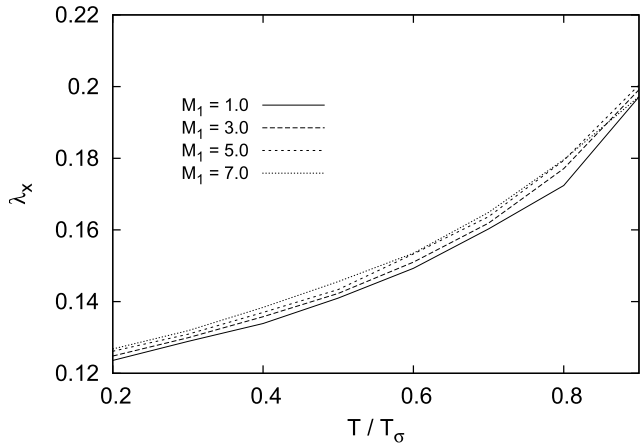

Figure 8. Temperature dependence of the theoretical penetration depth for different values of the coupling parameter M_1. Parameter $b = 0.01$ and other parameter values are the same as in figure 1.

$\lambda_{ab} \approx 900$ Å while the theoretically calculated value for MgB_2 in the clean limit is $\lambda_{ab} \approx 400$ Å [32]. This theoretically calculated value is in accordance with the isotropic H_{c1} observed previously [33] and also with the SANS measurement [34]. The result obtained from the single gap model involving field dependent coherence length and penetration depth suggests a variation in the penetration depth value from $\lambda_{ab} \approx 450$ to 700 Å for low to high applied magnetic field. With the increase in the applied magnetic field the penetration depth increases due to the decrease in the superfluid density arising as a result of the destruction of superconductivity in the π-bands. It is thus evident that in the case of MgB_2 superconductor the determination of the penetration depth from the derivative of the reversible magnetization data, as has been carried out in [14], leads to a gross overestimation of λ_{ab} if the magnetic field dependence of coherence length and penetration depth is not taken into account. In our present work instead of determining the penetration depth from the derivative of reversible magnetization we have calculated it directly from the magnetic field profile. As can be seen from the figure the results obtained by our theoretical calculation indicate a penetration depth of $\lambda_{ab} < 900$ Å. In the higher magnetic field regime our results are in accordance with those obtained by Klein *et al* [22], while the discrepancy increases with the decrease in the magnetic field induction due to the enhanced dominance of the three-dimensional π-band in the lower magnetic field regime. The inset of figure 6 shows that the inverse square of the penetration depth decreases with increasing field and almost saturates at higher field. This is in contrast to the result of linear dependence of the penetration depth on the magnetic field as reported earlier [22].

Figure 7 shows the comparison of the analytical temperature dependence of the penetration depth with the experimental data of MgB_2 [32]. The behaviour of the theoretical results and experimental data is qualitatively the same. At low temperature the theoretical result is limited by the limitation of the applicability of the GL theory. The temperature dependence of the penetration depth of the system, however, shows a great effect with the change in the parameter M_1, as can be seen from figure 8. With increase in the gradient coupling parameter M_1 there is slight increase in the penetration depth at all temperatures.

Figure 9 shows the plot of the magnetic form factor computed analytically with that obtained from the SANS measurements. The magnetic field inductions are measured in terms of the upper critical field corresponding to the dominant σ-band order parameter component (i.e. $b = \bar{B}/H_{c2}$, where H_{c2} is the upper critical magnetic field corresponding to the σ-band order parameter component). Over a wide range of the applied magnetic field regime the analytical results show very good agreement with the experimental data. The disagreement in the low magnetic field regime is expected as our two-dimensional model is not suitable for low applied field due to the increased dominance of the three-dimensional π-band in that regime.

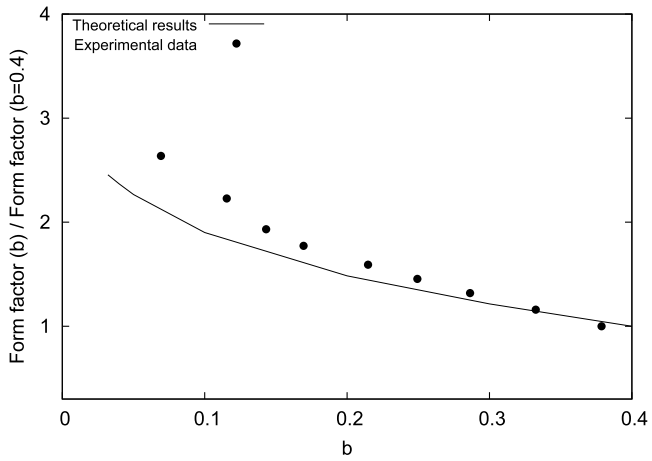

Figure 9. A comparison between the theoretical magnetic form factor and experimental data [22]. The other parameter values are the same as in figure 1.

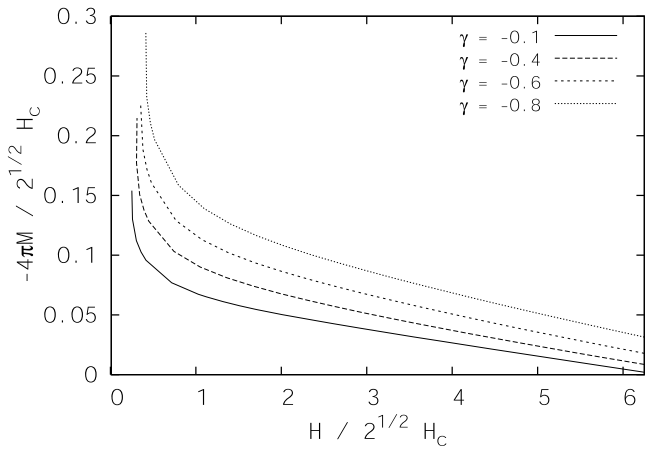

Figure 10. Reversible magnetization versus applied field plot for different values of the linear interband coupling parameter γ. The other parameter values are the same as in figure 1.

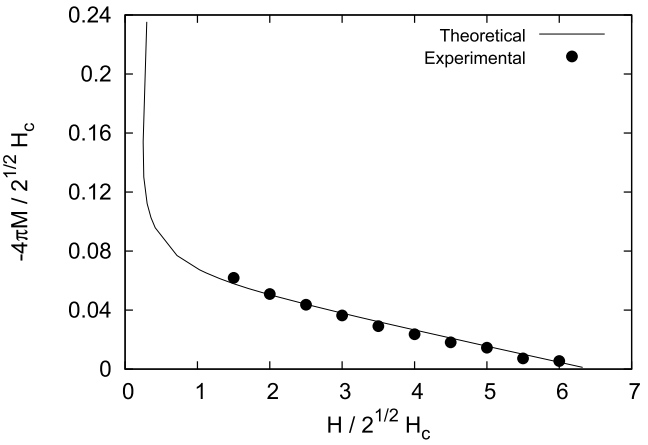

Figure 11. A comparison between the theoretical reversible magnetization and experimental data for MgB_2 [28]. The other parameter values are the same as in figure 1.

3.3. Reversible magnetization

Earlier theoretical models [23], which used an effective single-order parameter GL theory to explain the reversible magnetization of MgB_2, have proved to be inadequate. The determination of the penetration depth of MgB_2 using the derivative of the reversible magnetization also leads to a gross overestimation of its value [14, 22]. We provide an accurate computation of the reversible magnetization. The reversible magnetization of the system is defined as $M = \bar{B} - H$, where the equilibrium applied magnetic field H is given by $H = 4\pi(\partial f/\partial \bar{B})$. Determination of H requires a numerical derivative of the free energy density functional f which is difficult to calculate numerically and is a possible source of error in the earlier reported analytical results of the reversible magnetization. A more convenient and accurate way is to use the virial theorem earlier developed by the authors for the two-order parameter GL theory [24], and the same approach has been used here to compute the reversible magnetization.

Using virial theorem the equilibrium applied magnetic field H for MgB_2 can be written as [24],

$$2H\bar{B} = \langle \omega_\sigma - \alpha\omega_\pi - \omega_\sigma^2 - 2\beta_\pi\omega_\pi^2 - 2\gamma\cos(\phi)(\omega_\sigma\omega_\pi)^{1/2} + 2B^2\rangle. \quad (3)$$

Using this expression and the relation $M = \bar{B} - H$ the reversible magnetization can be calculated for various values of the coupling parameter γ. The result is shown in figure 10. The magnitude of the reversible magnetization shows marked changes with change in the parameter γ though the behaviour remains qualitatively the same. Figure 11 shows a comparison between the experimental data [28] of the reversible magnetization and our analytical results. The match between the two is excellent. From the best fit of the analytical reversible magnetization data with the experiment we obtain the value of the only free parameter in our model $\gamma = -0.1$. We have used this value of the parameter $\gamma = -0.1$ for all our analytical calculations. A comparison between the experimental data [28] and the theoretically computed temperature dependence of the reversible magnetization of the system for the applied magnetic field range $0.1\,\mathrm{T} \leqslant H \leqslant 2.0\,\mathrm{T}$ is presented in figure 12. The fitting between the theoretical and experimental data has been carried out using the Clem and Hao method [35]. The curves systematically shift towards the left with the increase in the applied magnetic field. Similar shifting in the reversible magnetization curves has also been observed in the case of conventional [36] as well as layered superconductors [37]. The match between the theoretical and experimental results is very good.

3.4. Current density

One of the principle reasons that has made MgB_2 one of the most studied superconducting materials of recent times is its high current carrying capacity in spite of its comparatively simple structure. The current density is related to the penetration depth as $|\mathbf{j}_c(T)| \approx 1/\lambda^2(T)$ [38]. Therefore, the current density also depends crucially on the details of the spatial behaviour of the order parameter components and the magnetic induction. Figure 13 shows the magnetic

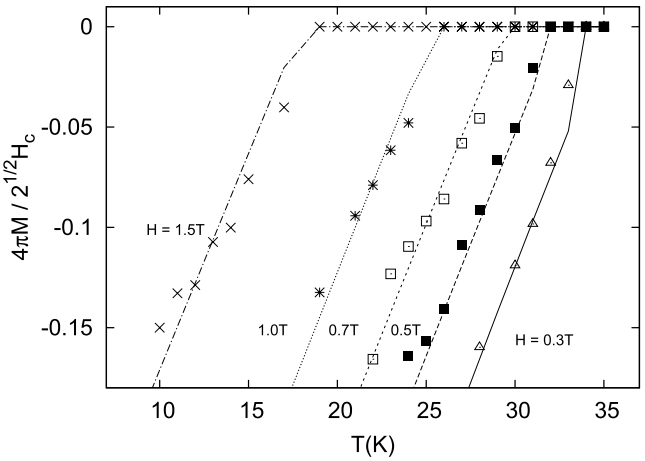

Figure 12. A comparison between the theoretical temperature dependence of the reversible magnetization and experimental data [28] for MgB_2. The other parameter values are the same as in figure 1.

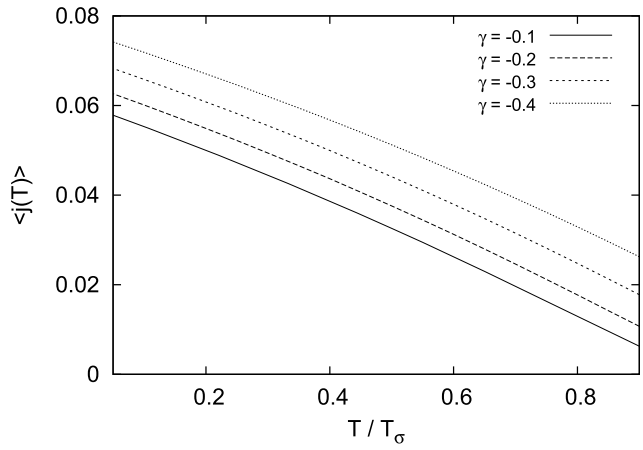

Figure 14. Temperature dependence of the theoretical superconducting current density for different values of the linear interband coupling parameter γ. Parameter $b = 0.01$ and the other parameter values are the same as in figure 1.

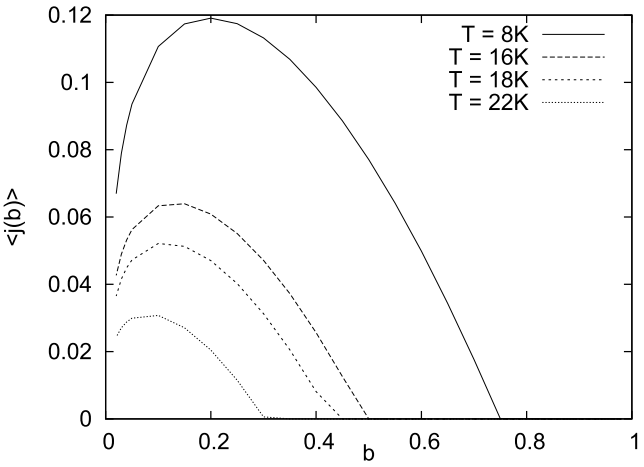

Figure 13. Variation of the theoretical supercurrent density with magnetic field induction for different temperatures. Parameter values used are the same as in figure 1.

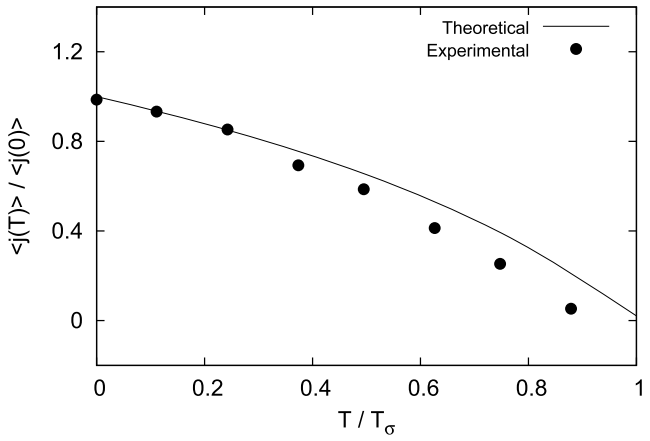

Figure 15. Comparison between the theoretical temperature dependence of the supercurrent density with the experimental data for MgB_2 [41]. Parameter $b = 0.003$ and the other parameter values are the same as in figure 1.

field dependence of the average current density at different temperatures. It can be seen that the magnitude of the current density is higher at lower temperature and at lower temperature the current can be carried over a wider range of applied magnetic field. Our analytical current density profile can be compared to the one obtained experimentally by Nishida *et al* [39]. Though the shape of the profile is the same in both the cases, an exact match is not expected since the experimental data correspond to MgB_2 thin films while our theoretical results correspond to bulk material. The experimental results also show a drop in the current density at low magnetic field, indicating that the sample is almost pin free as compared to cuprates [40]. Figure 14 shows the temperature dependence of the average current density for different values of the interband coupling parameter γ. The figure shows significant variation in the current density with the magnitude of the current density decreasing with increasing value of γ. This is due to the fact that the penetration depth increases with increasing interband coupling parameter γ which is also observed from our analytical calculation of the penetration depth. Figure 15 shows the best fit of the analytical result computed at very low applied field ($H \approx 0.0084$ T) with the experimental data [41]. The match between the theoretical and experimental results is quite good and the discrepancy can be attributed to the fact that the theoretical calculation is carried out at low magnetic field where the two-dimensional theoretical model ceases to be accurate due to the increasing contribution of the three-dimensional π-band to superconductivity, as mentioned above.

3.5. Shear modulus (c_{66}) of the vortex lattice

The shear modulus (c_{66}) of the vortex lattice gives a measure of the stability of the vortex lattice against the melting of the flux line lattice due to thermal fluctuations. Even though the effect of thermal fluctuation is not so prominent in MgB_2 superconductors as in cuprates, recent studies have shown that the phenomenon of vortex lattice melting is still important for

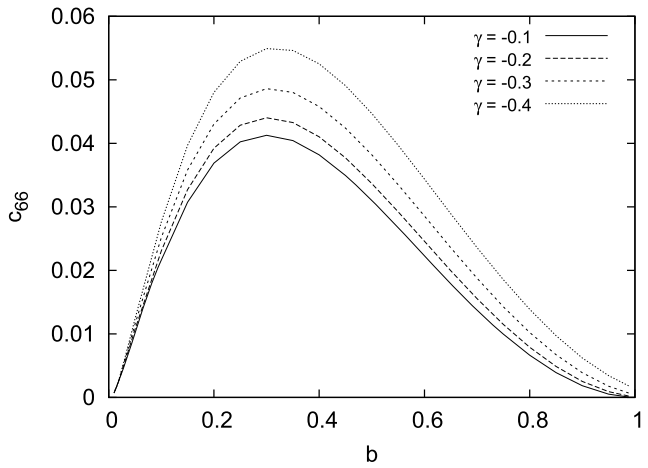

Figure 16. Magnetic field dependence of the shear modulus (c_{66}) of the vortex lattice corresponding to different values of the linear interband coupling parameter γ. The other parameter values are the same as in figure 1.

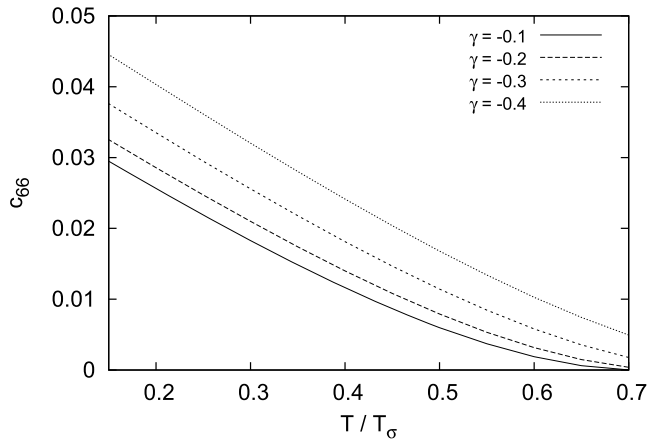

Figure 17. Temperature dependence of the shear modulus (c_{66}) of the vortex lattice for different values of the linear interband coupling parameter γ. Parameter $b = 0.3$ and the other parameter values are the same as in figure 1.

MgB_2 [25]. The shear modulus of the vortex lattice can be defined as the difference in the free energy density between a rectangular and a triangular lattice

$$c_{66} = 2\pi^2[y_2(\gamma)/x_1]^2[f(x_2 = 0, y_2(\gamma)) - f(x_2 = x_1/2, y_2(\gamma))] \quad (4)$$

where x_1, x_2 and y_2 are vortex lattice parameters which determine the shape of the vortex lattice. The parameter $y_2(\gamma)$ thus determines the interband coupling parameter dependence on the shape of the vortex lattice.

Figure 16 shows the magnetic field dependence of the shear modulus (c_{66}) of the vortex lattice for different values of the linear interband coupling parameter γ. For any value of the coupling parameter γ, the shear modulus of the vortex lattice increases, reaches a maximum and subsequently decreases with the increase in the magnetic field induction b. A positive value of the shear modulus of the vortex lattice (c_{66}) indicates that the corresponding symmetry of the vortex lattice is stable. It can be seen from the figure that though the behaviour remains qualitatively the same for all values of the linear interband coupling parameter γ, the magnitude varies significantly, indicating the effect of the interband coupling parameter γ. A decrease in the coupling parameter γ enhances the magnitude of the shear modulus (c_{66}) of the vortex lattice. In other words, an enhanced interband coupling leads to the softening of the vortex lattice. The observation is consistent with the variation of penetration depth of the system with the coupling parameter γ as obtained from our calculations. A careful observation of the variation of the width of the magnetic field profile $B(x, 0)$ for different values of the coupling parameters γ suggests a dependence of the form $1/\lambda^2 \approx c_{66}$.

Figure 17 shows the temperature dependence of the shear modulus of the vortex lattice of MgB_2 superconductor. It can be seen from the figure that for a given value of magnetic field induction b the shear modulus (c_{66}) of the vortex lattice decreases with the increasing temperature indicating that the melting of the vortex lattice is favoured at high temperature. The observation is in accordance with the experimental observations of melting of the vortex lattice of MgB_2 [25]. Also, a higher linear interband coupling results in a smaller shear modulus of the vortex lattice, i.e. a softening of the vortex lattice is favoured in this case. The observation is again in accordance with the current density behaviour observed from figure 14, which suggests that a higher interband coupling which favours the melting of the vortex lattice indeed supports a smaller current density.

4. Summary and conclusions

We have studied the spatial distribution of the order parameters and magnetic field induction and their variation with temperature and applied magnetic field. The study has been motivated by the experimental observations of anomalous magnetic field dependence of the various properties of the MgB_2 superconductor. We have used a two-order parameter GL theory to take into account the two-band nature of MgB_2. The nonlinear GL equations are solved using a numerically exact iteration method over the entire range of applied magnetic field, wide range of temperature and arbitrary vortex lattice symmetry. The spatial distribution of the order parameters reveals two different spatial length scales for the two bands, in agreement with the recent STM experiments on MgB_2. This provides an interesting vortex core structure, the π-band having a larger vortex core size as compared to that of the σ-band. The effect of the two spatial length scales and the linear interband coupling parameter γ significantly affects the properties of MgB_2. On the contrary, there is very little effect of the mixed gradient coupling parameter on the properties of MgB_2. Our computation of the magnetic field dependence of the penetration depth directly from the spatial profile of the magnetic induction provides better results than the one determined by using the derivative of reversible magnetization [14] which leads to an overestimation of λ_{ab}. This is important since the penetration depth is related to several other properties of the system. This interesting

observation suggests that, unlike the case of tetragonal high-T_c cuprates in which the mixed gradient coupling term plays a decisive role, for MgB_2 it is the linear interband coupling parameter γ that is important. We have shown that both the vortex core radius and the penetration depth are applied magnetic field dependent and this is due to the change in supercarrier density as superconductivity in the π-band is suppressed by the applied field. The calculated vortex core radius and the magnetic form factor which depends on the spatial behaviour of the order parameters and the magnetic field distribution show good agreement with the experiment. The vortex lattice configuration for MgB_2 as obtained from our isotropic two-order parameter GL model is triangular, an observation which is supported by previous experimental results [29, 11]. We have, however, not observed the 30° orientation of the vortex lattice, as observed in some of the recent neutron scattering experiments [11]. Such anisotropy of the vortex lattice can be attributed to the anisotropy of the σ- and π-bands which favours different vortex lattice orientations. At low fields the vortex lattice orientations will be dominated by screening currents on the π-band while at higher fields it is the σ-band which determines the vortex lattice structure. Theoretically such an orientation in the vortex lattice can be observed in the case where we incorporate higher-order gradient terms in our free energy density functional [20]. The calculated reversible magnetization shows excellent agreement with the experimental data over the entire range of the applied field. For accurate computation of the reversible magnetization we made use of the virial theorem, which avoids taking the numerical derivative of the free energy density functional which gives inaccurate results. The calculated superconducting current density and its dependence on applied magnetic field and temperature shows good match with the experimental results. The calculated variation of the current density and the shear modulus of the vortex lattice with the linear interband coupling parameter γ are consistent with the melting of the flux line lattice. Our results show that in the case of a softer vortex lattice, which favours its melting, the current carrying capacity of the material is indeed reduced.

An interesting problem would be to extend the model by taking into consideration the three-dimensional nature of the system to take care of the lower magnetic field regime. This can be done by considering the thin film geometry of the superconductor [42] and study in this direction is in progress.

Acknowledgments

The authors would like to thank UGC, India and BCUD, University of Pune, Pune for financial assistance. One of the authors (MK) would like to thank M N Kunchur and J J Betouras for fruitful discussions.

References

[1] Nagamatsu J, Nakagawa N, Muranaka T, Zenitani Y and Akimatsu J 2001 *Nature* **410** 63
[2] Giubileo F, Roditchev D, Sacks W, Lamy R, Thanh D X, Klein J, Miraglia S, Fruchart D, Marcus J and Monod Ph 2001 *Phys. Rev. Lett.* **87** 177008
[3] Iavarone M, Karapetrov G, Koshelev A E, Kwok W K, Crabtree G W, Hinks D G, Kang W N, Choi E-M, Kim Hyun J, Kim H-J and Lee S I 2002 *Phys. Rev. Lett.* **89** 187002
[4] Bud'ko S L, Lapertot G, Petrovic C, Cunningham C E, Anderson N and Canfield P C 2001 *Phys. Rev. Lett.* **86** 1877
[5] Suhl H, Matthias B T and Walker L R 1959 *Phys. Rev. Lett.* **3** 552
[6] Choi H J, Roudny D, Sun H, Cohen M L and Louie S G 2002 *Nature* **418** 758
[7] Pissas M, Papavassiliou G, Karayanni M, Fardis M, Maurin I, Margiolaki I, Prassides K and Christides C 2002 *Phys. Rev.* B **65** 184514
Papavassiliou G, Pissas M, Fardis M, Karayanni M and Christides C 2002 *Phys. Rev.* B **65** 012510
[8] Jin R, Paranthaman M, Zhai H Y, Christen H M, Christen D K and Mandrus D 2001 *Phys. Rev.* B **64** 220506(R)
[9] Lyard L *et al* 2002 *Phys. Rev.* B **66** 180502(R)
Bud'ko S L, Kogan V G and Canfield P C 2001 *Phys. Rev.* B **64** 180506
Angst M, Puzniak R, Wisniewski A, Jun J, Kazakov S M, Karpinski J, Roos J and Keller H 2002 *Phys. Rev. Lett.* **88** 167004
Welp U *et al* 2003 *Phys. Rev.* B **67** 012505
[10] Szabo P *et al* 2001 *Phys. Rev. Lett.* **87** 137005
Samuely P *et al* 2003 *Physica* C **385** 244
[11] Cubitt R, Eskildsen M R, Dewhurst C D, Jun J, Kazakov S M and Karpinski J 2003 *Phys. Rev. Lett.* **91** 047002
[12] Kunchur M, Saracila G, Arcos D A, Cui Y, Pogrebnyakov A, Orgiani P, Xi X X, Adams P W and Young D P 2006 *Physica* C **437/438** 171–5
[13] Bouquet F, Wang Y, Sheikin I, Plackowski T, Junod A J, Lee S and Tajima S 2002 *Phys. Rev. Lett.* **89** 257001 and the references therein
[14] Angst M, DiCastro D, Eschenko D G, Khasanov R, Kohout S, Savic I M, Shengelaya A, Budko S L, Canfield P C, Jun J, Karpinski J, Kazarov S M, Ribeiro R A and Keller H 2004 *Phys. Rev.* B **70** 224513
[15] Giubileo F, Roditchev D, Sacks W, Lamy R and Klein J K 2002 *Europhys. Lett.* **58** 764
[16] An J M and Pickett W E 2001 *Phys. Rev. Lett.* **86** 4366
[17] Hirsh J E 2001 *Phys. Lett.* A **282** 392
Hirsh J E and Marsiglio F 2001 *Phys. Rev.* B **64** 144523
Belashchenko K D, Antropov V P and Rashkeev S N 2001 *Phys. Rev.* B **64** 132506
Joas C, Eremin I, Manske D and Bennemann K H 2002 *Phys. Rev.* B **65** 132518
Ivanov V A, van den Broek M and Peeters F M 2001 *Soild State Commun.* **120** 53
Posazhennikova A I, Dahm T and Maki K 2002 *Europhys. Lett.* **60** 134
[18] Baskaran G 2002 *Phys. Rev.* B **65** 212505
Yamaji K 2001 *J. Phys. Soc. Japan* **70** 1476
[19] Koshelev A E and Golubov A A 2003 *Phys. Rev. Lett.* **90** 177002 and the references therein
[20] Zhitomirsky M E and Dao V H 2004 *Phys. Rev.* B **69** 054508
[21] Betouras J J, Ivanov V A and Peeters F M 2003 *Eur. Phys. J.* B **31** 349
[22] Klein T, Lyard L, Marcus J, Holanova Z and Marcenat C 2006 *Phys. Rev.* B **73** 184513
[23] Zehetmeyer M, Eisterer M, Jun J, Kazakov S M, Karpinski J and Weber H W 2004 *Phys. Rev.* B **70** 214516
[24] Karmakar M and Dey B 2006 *Phys. Rev.* B **74** 172508
[25] Nie Q-M, Lv J-P and Chen Q-H 2010 *Phys. Lett.* A **374** 655–8
[26] Gurevich A and Vinokour V M 2003 *Phys. Rev. Lett.* **90** 047004
[27] Doh H, Sigrist M, Cho B K and Lee S-I 1999 *Phys. Rev. Lett.* **83** 5350
[28] Kang B, Kim H-J, Park M-S, Kim K-H and Lee S-I 2004 *Phys. Rev.* B **69** 144514

[29] Dahm T and Schopohl N 2003 *Phys. Rev. Lett.* **91** 017001
Eskildsen M R, Kugler M, Tanaka S, Jun J, Kazakov S M, Karpinski J and Fischer ø 2002 *Phys. Rev. Lett.* **89** 187003
[30] Graser S, Gumann A, Dahm T and Schopohl N 2007 *Physica* C **460–462** 564–5
[31] Gumann A, Graser S, Dahm T and Schopohl N 2006 *Phys. Rev.* B **73** 104506
[32] Golubov A A, Brinkman A, Dolgov O V, Kortus J and Jepsen O 2002 *Phys. Rev.* B **66** 054524
[33] Lyard L, Szabo P, Klein T, Marcus J, Marcenat C, Kim K H, Kang B W, Lee H S and Lee S I 2004 *Phys. Rev. Lett.* **92** 057001
[34] Pal D, De Beer-Schmitt L, Bera T, Cubitt R, Dewhurst C D, Jun J, Zhigadlo N D, Karpinski J, Kogan V G and Eskildsen M R 2006 *Phys. Rev.* B **73** 012513
[35] Hao Z, Clem J R, McElfresh M W, Civale L, Malozemoff A P and Holtzberg F 1991 *Phys. Rev.* B **43** 2844
[36] Suenaga M, Ghosh A K, Xu Y and Welch D O 1991 *Phys. Rev. Lett.* **66** 1777
[37] Kim M-S, Lemberger T R, Jung C U, Choi J-H, Kim J Y, Kim H-J and Lee S-I 2002 *Phys. Rev.* B **66** 214509
[38] Askerzade I N 2003 *Physica* C **390** 281–5
[39] Nishida A, Taka C, Chromik S and Durny R 2005 *Physica* C **426–431** 340–4
[40] van-der Beek C J, Konczykowski M, Abal'oshev A, Abal'osheva I, Gierlowski P, Lewandowski S J, Idenbom M V and Barbanera S 2002 *Phys. Rev.* B **66** 024523
[41] Sahin H and Askerzade I N 2007 *Eur. Phys. J. Appl. Phys.* **36** 267–70
[42] Brandt E H 2005 *Phys. Rev.* B **71** 014521